ornl.gov/grailexp/) was used to build gene models from a combination of EST/mRNA alignments and computationally predicted exon candidates. The databases used in the gene modeling process include RefSeq, TIGR EGAD, the Baylor Human Transcript database, the Univ. of Penn. Database of Transcribed Sequences (DOTS), and Dbest. Genscan (http://genes.mit.edu/GENSCAN.html) was also run on the sequences (after repeat-masking). Because Genscan does not use integrated ESTs or reference gene message information, the gene models generated with this program were not allowed to cross a sequence gap.

9. The global comparative analysis of the assembled human contigs was carried out with NCBI's blastall version 2.0.14 program (*43*). Contigs were masked for simple sequence and repeats with RepeatMasker (http://ftp.genome.washington.edu/cgi-bin/RepeatMasker/) and then used to search syntenically homologous mouse BAC clones (using blastn and tblastx) and a series of other data sets including NCBI's EST and nonredundant databases (7 October 2000 release, using blastn), and *Drosophila*, *C. elegans*, and yeast amino acid sequence databases (7 October 2000 release; using tblastx). All BLAST matches with e scores less than 10^{-2} were collected, parsed, merged and then used to define "sequence feature blocks" on the basis of overlapping hits. Locus Link, unigene, and IMAGEne IDs were retrieved for all relevant matching human accession numbers. All information was entered into a database for statistical queries and the generation of graphical views. A display of these combined data sets is available on http://bahama.jgi-psf.org/pub/ch19.
10. Web figure and tables are available on *Science* Online at www.sciencemag.org/cgi/content/full/293/5527/104/DC1.
11. Repeat and GC content of 200 kb assembled human fragments and mouse BACs was determined with RepeatMasker (http://ftp.genome.washington.edu/cgi-bin/RepeatMasker/).
12. J. L. Gao *et al.*, *Genomics* **51**, 270 (1998).
13. D. R. Nelson, *Arch. Biochem. Biophys.* **369**, 1 (1999).
14. HSA19 and mouse regions were used as query sequence in a BLAST search against themselves. Results were parsed, self-hits were eliminated, and a graph was created such that each HSA19 or mouse region represents a node and any hit between two regions constitutes an edge whose weight is equal to the e score. For each gene family, an appropriate maximum e score was chosen and all connected nodes found. E scores were chosen by incrementally raising the threshold until groupings for that family were obviously incorrect. For KRABA, ZNF, OLFR, and VNO, the e scores chosen were e^{-60}, e^{-75}, e^{-20}, and e^{-15}, respectively. Different e scores reflect relative conservation between members of the family. In KRAB-ZNF genes, the KRABA and zinc-finger domains are each encoded by single exons (*13*), so that there is a one-to-one correspondence between sequence feature blocks containing these elements and individual genes. Because each sequence feature block generally contains only one exon or exon fragment, only single exons of multiexon genes are found; therefore, for other ZNF gene types that contain more than one finger domain, the gene count will be an overestimate. Likewise, OR (*18*) and VR1 (*23*) coding sequences are contained within a single exon, simplifying the analysis of these genes. VR2 genes have a more complex structure; to identify these genes and assess coding capacity, we focused on the analysis of sequences in a single exon encoding the conserved membrane spanning domains (*24*). To find exon fragments, such as the numerous pseudogene fragments found for VR1 and VR2 genes in HSA19, we set the e scores to be relatively high; this caused an increase in the number of false positives. Resulting sets of matches corresponding to all families were therefore examined by hand to determine validity of membership and coding capacity. Details of each hit and tables summarizing the locations and properties of each gene set are summarized in Web tables B through G.
15. E. J. Bellefroid *et al.*, *Proc. Natl. Acad. Sci. U.S.A.* **88**, 3608 (1991).
16. A multiple alignment of the HSA19 and syntenic mouse KRABA nucleotide sequence was created with ClustalX (*44*). Using PHYLIP (*45*), we generated a consensus distance tree using dnadist, neighbor, and consense programs with 1000 rounds of bootstrapping. The results of this procedure are consensus trees and branch lengths therefore do not represent distance; however, the topology of the tree correctly shows relationships between the groups. Details of the KRAB sequences used in the tree are summarized in Web tables D and E.
17. M. Abrink *et al.*, *Proc. Natl. Acad. Sci. U.S.A.* **98**, 1422 (2001).
18. M. Shannon, L. Stubbs, *Genomics* **49**, 112 (1998).
19. P. Mombaerts, *Science* **289**, 707 (1999).
20. M. Shannon, L. Stubbs, unpublished data.
21. S. Roquier, A. Blancher, D. Giorgi, *Proc. Natl. Acad. Sci. U.S.A.* **97**, 2870 (2000).
22. M. Lapidot *et al.*, *Genomics* **71**, 296 (2001).
23. S. Sullivan *et al.*, *Proc. Natl. Acad. Sci. U.S.A.* **93**, 884 (1996).
24. C. Dulac, R. Axel, *Cell* **83**, 195 (1995).
25. J. Kim, manuscript in preparation.
26. H. Matsunami, L. Buck, *Cell* **90**, 775 (1997).
27. I. Rodriguez *et al.*, *Nature Genet.* **26**,18 (2000).
28. D. Giorgi *et al.*, *Genome Res.* **10**, 1979 (2000).
29. F. Richard *et al.*, *Genome Res.* **10**, 644 (2000).
30. P. Dehal *et al.*, data not shown.
31. E. Ostrander, F. Galibert, D. Patterson, *Trends Genet.* **16**, 117 (2000).
32. W. J. Murphy *et al.*, *Genome Res.* **10**, 691 (2000).
33. M. Band *et al.*, *Genome Res.* **10**, 1359 (2000).
34. J. H. Postalthwait *et al.*, *Genome Res.* **10**, 1890 (2000).
35. We examined all alignments in the duplicated region that were more than 500 bp in length and were not part of the *Pdxk* or *Notch3* genes or repetitive elements. The duplication date was estimated by multiplying the total percent identity (89.5%) over all aligned segments (10.7 kb) and dividing the percent difference (10.5%) number by the estimated neutral mutation rate for mouse, as determined by Li and colleagues (*46*).
36. Y. Ji *et al.*, *Genome Res.* **10**, 597 (2000).
37. E. Carver, L. Stubbs, *Genome Res.* **7**, 1123 (1997).
38. K. A. Frazer *et al.*, *Nature Genet.* **9**, 424 (1995).
39. M. Lynch, J. S. Conery, *Science* **290**, 1151 (2000).
40. T. L. Hawkins *et al.*, *Nucleic Acids Res.* **22**, 4543 (1994).
41. B. Ewing *et al.*, *Genome Res.* **8**, 175 (1998).
42. X. Huang, *Genomics* **33**, 21 (1996).
43. S. F. Altschul *et al.*, *Nucleic Acids Res.* **25**, 3389 (1997).
44. J. D. Thompson *et al.*, *Nucleic Acids Res.* **24**, 4876 (1997).
45. J. Felsenstein, Phylogeny Inference Package, version 3.5 (University of Washington, Seattle, WA, 1993).
46. R. Puttagunta *et al.*, *Genome Res.* **10**, 1369 (2000).
47. We thank the staff of the JGI sequencing team for an outstanding effort; a complete list of contributors can be found at photo http://bahama.jgi-psf.org/pub/ch19/people.html. We were provided useful technical discussions and critical comments on the manuscript by J. Boore, B. Wold, and M. Frazier. This research was performed under the auspices of the U.S. Department of Energy at Lawrence Livermore National Laboratory under contract W-7405-Eng-48, Lawrence Berkeley National Laboratory under contract DE-AC03-76SF00098, (managed by the University of California), and Oak Ridge National Laboratory under contract DE-AC05-00OR22725 (managed by UT-Battelle, LLC).

28 February 2001; accepted 1 June 2001

Ventroptin: A BMP-4 Antagonist Expressed in a Double-Gradient Pattern in the Retina

Hiraki Sakuta,[1] Ryoko Suzuki,[1,3] Hiroo Takahashi,[1,3] Akira Kato,[1,3] Takafumi Shintani,[1,3] Shun-ichiro Iemura,[2] Takamasa S. Yamamoto,[2] Naoto Ueno,[2,3] Masaharu Noda[1,3]*

In the visual system, the establishment of the anteroposterior and dorsoventral axes in the retina and tectum during development is important for topographic retinotectal projection. We identified chick Ventroptin, an antagonist of bone morphogenetic protein 4 (BMP-4), which is mainly expressed in the ventral retina, not only with a ventral high–dorsal low gradient but also with a nasal high–temporal low gradient at later stages. Misexpression of *Ventroptin* altered expression patterns of several topographic genes in the retina and projection of the retinal axons to the tectum along both axes. Thus, the topographic retinotectal projection appears to be specified by the double-gradient molecule Ventroptin along the two axes.

Axonal connection patterns in the nervous system often form topographic maps, with nearest neighbor relationships of the projection neurons maintained in their connections within the target. The projection from the retina to the tectum is a good model system for understanding the development of topographic maps. Graded distributions of topographic molecules along the anteroposterior (A-P) (nasotemporal) and dorsoventral (D-V) axes in the retina and tectum, which are derived from the regional specialization along the two axes during retinal and tectal development, control the topographical projection of retinal axons (*1*). Although gradients of diffusible factors and transcription factors are known to control the regional specificities in the retina during development (*2–6*), the molecular mechanisms involved are mostly unknown. We performed large-scale screening of region-specific molecules (*7*) [also see supple-

[1]Division of Molecular Neurobiology, National Institute for Basic Biology, [2]Division of Morphogenesis, National Institute for Basic Biology, [3]Department of Molecular Biomechanics, The Graduate University for Advanced Studies, 38 Nishigonaka, Myodaiji-cho, Okazaki 444-8585, Japan.

*To whom correspondence should be addressed. E-mail: madon@nibb.ac.jp

mental Web information (*8*)], using a new cDNA display system: restriction landmark cDNA scanning (RLCS) (*9*). We found a molecule that has activity to antagonize the function of bone morphogenetic protein 4 (BMP-4).

Figure 1A shows corresponding parts of a pair of RLCS profiles for the dorsal and ventral retina when Bam HI was used as the first restriction enzyme. The cDNA fragment corresponding to the ventral-specific spot shown with an arrow in Fig. 1A (tentatively named V/Bam HI 1) was recovered from the gel and was subcloned into a plasmid for further analysis. Northern blotting using this fragment as a probe revealed a single 4.9-kb transcript in the ventral retina at embryonic day 8 (E8) (Fig. 1B). This molecule was repeatedly identified not only as ventral-specific but as nasal-specific in our RLCS screening (*8*).

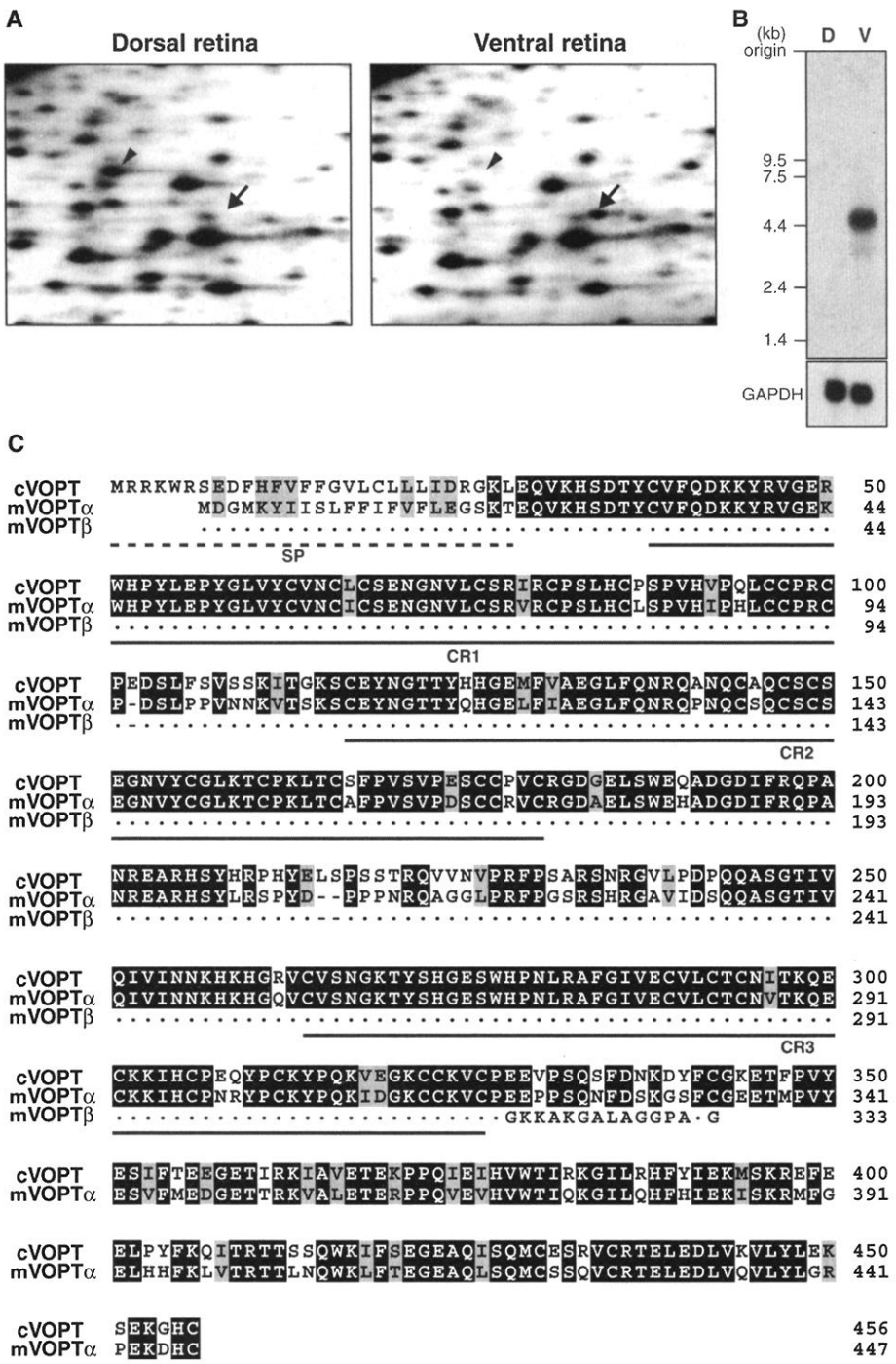

Fig. 1. Isolation of *Ventroptin* by the RLCS method. (**A**) RLCS profiles of the dorsal and ventral retina. The V/Bam HI 1 (Ventroptin) spot is indicated by an arrow. The spot with an arrowhead was retinaldehyde dehydrogenase 1 (*7*). (**B**) *Ventroptin* mRNA expression in the dorsal (D) and ventral (V) retina. RNA blot hybridization analysis (10 μg of total RNA per lane) was done using the cDNA fragment of V/Bam HI 1 as a probe. The dorsal or ventral one-third of the retina was used for RNA preparation for RLCS and RNA blotting. GAPDH, glyceraldehyde phosphate dehydrogenase. (**C**) Alignment of chick (cVOPT) and mouse (mVOPT) Ventroptin sequences. The Genetics Computer Group program PileUp was used. The locations of the putative signal peptide (SP) and three CRs are shown. Amino acids that are identical between chick and mouse are shadowed in black; those that are similar are shadowed in gray. Dashes indicate gaps. Dots indicate amino acids that are identical between mouse Ventroptin-α and mouse Ventroptin-β. Amino acid identity and similarity between chick Ventroptin and mouse Ventroptin-α are 80 and 86%, respectively.

Full-length V/Bam HI 1 clones isolated from an E8 chick retina cDNA library encoded a protein of 456 amino acids, with a putative signal peptide and three cysteine-rich repeats (CRs) (Fig. 1C; GenBank accession no. AF257352). CRs are characteristic motifs that are conserved in some proteins, including von Willebrand factor and Chordin. Here we refer to this molecule as Ventroptin (VOPT), after the place where it is mainly expressed. Ventroptin is likely to be a secretory protein, because it was found in culture supernatant prepared from chick embryonic fibroblasts (CEFs) infected with a recombinant expression virus vector for Ventroptin (RCAS/VOPT-flag) (*8*) as a single band of about 50 kD by Western blot analysis (*10*). This size coincides with the predicted molecular weight of the Ventroptin protein when processed at the signal sequence (Fig. 1C).

We cloned mouse *Ventroptin* cDNA to deduce the structure of the mouse ortholog (Fig. 1C) (*8*). Two splicing isoforms were found for mouse Ventroptin: a long form (Ventroption-α; accession no. AF321853) and a short form (Ventroption-β; accession no. AF296451). The β isoform was devoid of the region after the third CR, as compared with the chick counterpart and the α isoform (Fig. 1C). Online database screening also identified a partial sequence of the human gene (accession no. AL049176).

In the chick eye, *Ventroptin* expression was first detected in the optic vesicle at Hamburger-Hamilton stage 11 by reverse transcription polymerase chain reaction (*10*) and became evident in the ventral retina at stage 14 when the optic vesicle invaginates, when examined by in situ hybridization (Fig. 2A). *Ventroptin* expression became still more manifest at E3 (stage 16 to 17) (Fig. 2B), when retinal neurogenesis just begins (*11*), seemingly in a complementary pattern to that of *BMP-4* (Fig. 2C). Another BMP member, *BMP-7*, is ubiquitously expressed in the eye region (*12*). Figure 2D shows *Ventroptin* expression in the retina with a ventral high–dorsal low gradient at E8. This D-V graded expression pattern was observed until E14, peaking at E8 (*10*). At E3, *Ventroptin* showed a uniform expression along the A-P axis.

However, a nasal high–temporal low gradient expression pattern was detected first at E6 and became obvious at E8 (Fig. 2E). At this stage, *Ventroptin* showed a double-gradient expression profile along the two axes (Fig. 2, F and G). At E3, before the retinal lamination, *Ventroptin* expression was observed throughout the ventral retinal tissue (Fig. 2B, inset). However, at E8, when retinal lamination becomes defined, *Ventroptin*-positive cells were localized to the inner nuclear layer (Fig. 2, D and E). This is evident in the central retina, where the development is advanced. *Ventroptin* was also expressed in organs other than the retina (*13*).

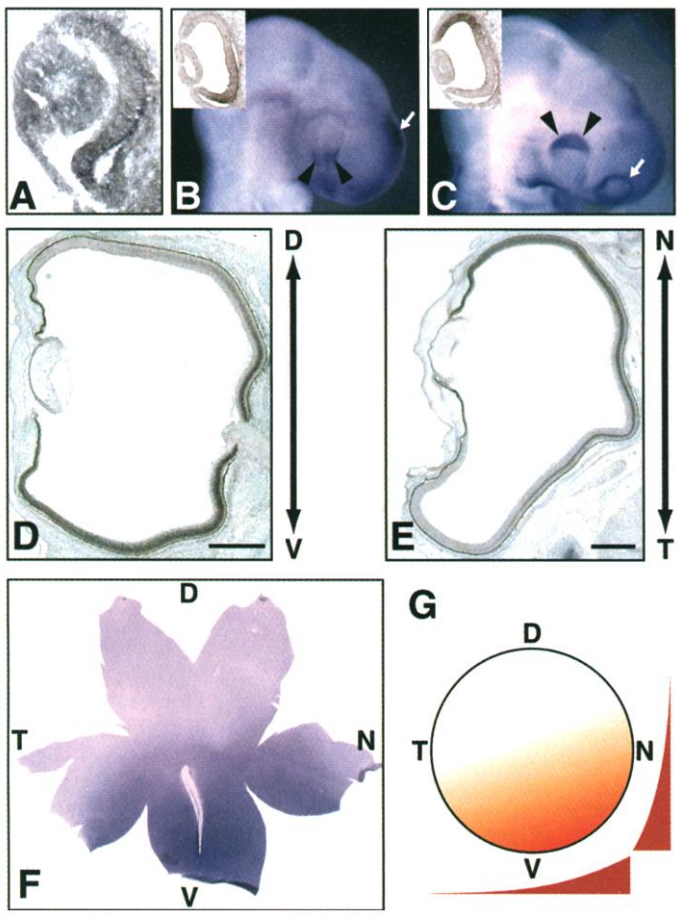

Fig. 2. Expression patterns of *Ventroptin* mRNA during development. (**A**) Coronal section in situ hybridization of the eye at stage 14. (**B** and **C**) Whole-mount in situ hybridization of E3 (stage 16 to 17) chick embryos for *Ventroptin* (B) and *BMP-4* (C). Insets show results in coronal sections of the E3 eyes. *Ventroptin* (B) was expressed in the ventral retina (arrowheads) and the forebrain (arrow). *BMP-4* (C) was expressed in the dorsal retina (arrowheads) and the periphery of the nasal pit (arrow). (**D**) Coronal section in situ hybridization at E8. *Ventroptin* is expressed in a ventral high–dorsal low (D ↔ V) gradient. (**E**) Horizontal section at E8. *Ventroptin* is expressed in a nasal high–temporal low (N ↔ T) gradient. (**F**) Flat-mount in situ hybridization of E8 retina. (**G**) Schematic drawing of *Ventroptin* expression in the retina. Double-gradient expression is represented by the density gradient of color. Scale bars, 600 μm in (D) and (E). N, T, D, and V indicate nasal, temporal, dorsal, and ventral, respectively.

Several secretory proteins that antagonize BMPs have been discovered to date (*14*): Noggin, Chordin, Follistatin, Cerberus, and Gremlin. These BMP antagonists specifically bind to BMPs and prevent their binding to specific receptors or their signaling. Because the three CRs of Ventroptin were significantly homologous with those of Chordin, although the remaining region has no homology, we speculated that Ventroptin binds to BMPs. Binding between Ventroptin and several transforming growth factor–β (TGF-β) family members was tested with a surface plasmon resonance biosensor. Ventroptin bound with high affinity to BMP-4 and with lower affinity to a BMP-4/7 heterodimer, but not at all to BMP-7, TGF-β, or activin [Web fig. 1A (*8*)]. Furthermore, BMP-4 is coimmunoprecipitated with Ventroptin [Web fig. 1B (*8*)].

The binding of Ventroptin to BMP-4 suggested that Ventroptin can inhibit BMP functions as Chordin does. We injected early *Xenopus* embryos with synthetic mRNA encoding chick Ventroptin [Web fig. 1C (*8*)]. Ventral expression of *Ventroptin* induced the formation of a secondary body axis in the injected embryos (in 66 out of 104 embryos). When *BMP-4* mRNA was coinjected, secondary axis formation induced by *Ventroptin* mRNA was completely repressed (in 57 out of 57 embryos), indicating that Ventroptin can bind to BMP-4 and inhibit its activity in vivo.

The dorsal retina-specific expression of *BMP-4* has been implicated in the dorsalization in the retina (*5*). However, no BMP-

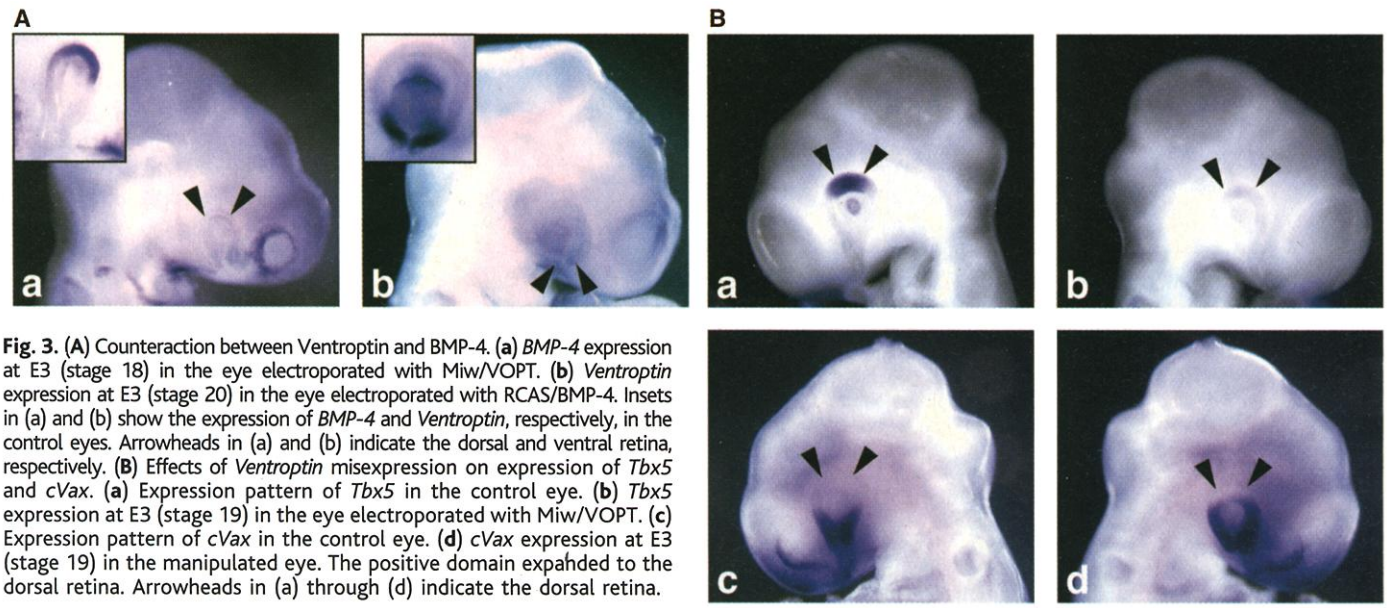

Fig. 3. (**A**) Counteraction between Ventroptin and BMP-4. (**a**) *BMP-4* expression at E3 (stage 18) in the eye electroporated with Miw/VOPT. (**b**) *Ventroptin* expression at E3 (stage 20) in the eye electroporated with RCAS/BMP-4. Insets in (a) and (b) show the expression of *BMP-4* and *Ventroptin*, respectively, in the control eyes. Arrowheads in (a) and (b) indicate the dorsal and ventral retina, respectively. (**B**) Effects of *Ventroptin* misexpression on expression of *Tbx5* and *cVax*. (**a**) Expression pattern of *Tbx5* in the control eye. (**b**) *Tbx5* expression at E3 (stage 19) in the eye electroporated with Miw/VOPT. (**c**) Expression pattern of *cVax* in the control eye. (**d**) *cVax* expression at E3 (stage 19) in the manipulated eye. The positive domain expanded to the dorsal retina. Arrowheads in (a) through (d) indicate the dorsal retina.

neutralizing factor has been identified in the retina so far: Neither *noggin* nor *chordin* was detected in the retina at E3 (stage 16 to 17) by in situ hybridization (*10*). The complementary expression patterns of *Ventroptin* and *BMP-4* [Fig. 2, B and C, and Web fig. 2 (*8*)] suggest that Ventroptin prevents BMP-4 from affecting the ventral part of the retina to ensure the ventral cell fate. Because these are secretory molecules, they are expected to diffuse for a distance and interact with each other. We thus tested the effects of misexpression of *Ventroptin* and *BMP-4* on each other's expression in the retina by in ovo electroporation [details are described in (*8*)]. This method allows us to express the transgenes almost uniformly in the retina [Web fig. 3 (*8*)]. When Miw/VOPT (*8*) was electroporated into the optic vesicle at stage 8 to 10, *BMP-4* expression was markedly reduced at E3 (stage 18 to 20) (Fig. 3A, a; 5 out of 7 embryos). On the other hand, misexpression of *BMP-4* repressed expression of *Ventroptin* (Fig. 3A, b; 7 out of 8 embryos). This is consistent with the findings that BMP-4 and its antagonists repress each other in early *Xenopus* embryos (*15*, *16*). These results suggest that Ventroptin and BMP-4 interact in vivo to keep their countergradient expression pattern along the D-V axis. There is a similar counteraction between Tbx5 and cVax (*4*, *5*).

Because BMP-4 is known to up-regulate *Tbx5* and down-regulate *cVax* (*5*), we tested the effects of misexpression of *Ventroptin* on *Tbx5* and *cVax* expression in the retina. After misexpression of *Ventroptin*, *Tbx5* expression was reduced (Fig. 3B, a and b; 11 out of 14 embryos) and *cVax* expression was induced (Fig. 3B, c and d; 8 out of 11 embryos) in the dorsal retina at E3 (stage 18 to 20). The extent of these phenotypes was correlated with the dose of the electroporated DNA (*10*).

Misexpression of *Tbx5* or *cVax* in the retina alters the pattern of projection of the retinal axons to the tectum along the D-V axis (*4*, *5*). Therefore, we analyzed retinotectal projections at E18 to E19 after misexpression of *Ventroptin*. To observe the behavior of the retinal ganglion cell axons, we labeled a small number of the dorsal retinal fibers with 1,1′-dioctadecyl-3,3,3′,3′-tetramethyl-indocarbocyanine perchlorate (DiI) (Fig. 4A, c) (*3*). In the control animals, the dorsal retinal axons converge at a terminal zone in the middle of the ventral tectum (asterisk) on the contralateral side (Fig. 4A, b and e; 12 out of 12 embryos). In embryos with misexpressed *Ventroptin* (Fig. 4A, a and d), in contrast, the dorsal axons did not form a tight terminal zone at the proper position (asterisk), and their trajectories shifted to the dorsal side in the ventral tectum (small arrows). Moreover, numerous axons projected to the dorsal tectum (large arrows) (9 out of 11 embryos): Three of nine embryos showed projections of dorsal axons only to the dorsal tectum. The axons did not stop in the middle of the tectum but extended to the posterior end (arrowheads in Fig. 4A, a). These results differ from those of ectopic expression of *cVax* in the dorsal retina, in which dorsal axons occasionally invade the dorsal tectum but never project beyond the middle of the tectum (*4*). To confirm mistargeting along the A-P axis, we also labeled the dorsotemporal axons. All these axons again overshot to the posterior end of the dorsal tectum in a manner similar to the dorsal axons (5 out of 5 embryos) (*10*, *17*). Therefore, aberrant projections in the embryos with misexpressed *Ventroptin* do not simply reflect the effect of dorsal induction of *cVax*.

The temporal high–nasal low gradient expression of EphA3 receptor in the retina is responsible for the topographic retinotectal projection along the A-P axis (*18*, *19*); and the nasal high–temporal low gradient of its

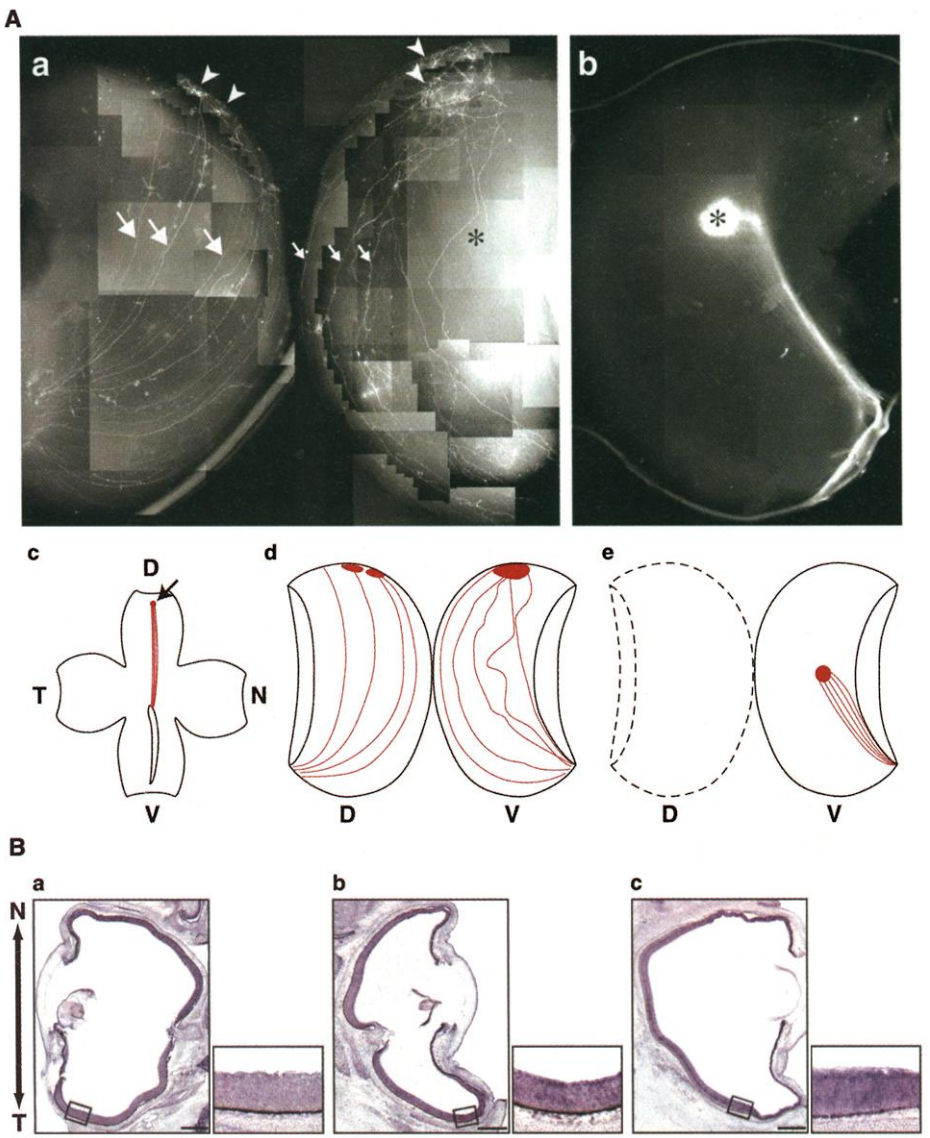

Fig. 4. (**A**) Retinotectal projection at E18 to 19 after simultaneous electroporation of Miw/VOPT and RCAS/VOPT. (**a**) A typical projection pattern in the embryo with misexpressed *Ventroptin*. Many dorsal axons shifted to the dorsal side (small arrows) or extended on the dorsal tectum (large arrows), and all the axons projected to the posterior end of the tectum (arrowheads). The asterisk indicates the proper terminal zone in the control embryo. (**b**) A typical projection pattern in the control embryo. The axons formed a tight terminal zone (asterisk) in the tectum. (**c**) The arrow indicates the position of the DiI label in the dorsal periphery of the right retina, close to the A-P midline. (**d** and **e**) Schematic drawings of (a) and (b), respectively. Anterior is down. (**B**) Effects of misexpression of *Ventroptin* and *noggin* on the expression of *ephrin A2*. (**a**) Control eye. *Ephrin A2* is not expressed in the temporal retina. (**b**) Eye transfected with Miw/VOPT and RCAS/VOPT. *Ephrin A2* expression was induced mainly in the ganglion cell layer in the E8 temporal retina. (**c**) Eye transfected with RCAS/Noggin. Ectopic *ephrin A2* expression was induced similarly. The right small panels in (a) through (c) are enlargements of the temporal areas boxed in the left panels. Scale bars, 600 μm. Nasal and temporal are top and bottom, respectively.

ligands, ephrins A2 and A5 in the retina, is involved in this process by modulating EphA receptor function (*20*, *21*). We examined the effect of *Ventroptin* misexpression on the expression patterns of these genes. Overexpression of *Ventroptin* induced expression of *ephrin A2* [which was not expressed in the temporal retina of the control eye (Fig. 4B, a)] in the temporal retina mainly in ganglion cells (Fig. 4B, b; 6 out of 6 embryos); whereas we did not detect any obvious alteration in the expression patterns of *EphA3* and *ephrin A5* (*10*). The ectopic projection of the dorsal and dorsotemporal axons to the caudal end of the tectum is explained by this *ephrin A2* induction: *Ephrin A2* overexpression in the retina possibly modified the signal transduction capacity of EphA receptors to make them insensitive to ephrins in the posterior tectum (*20*). *CBF-1*, *CBF-2*, *SOHo1*, and *GH6* are known to be involved in the retinal specification along the A-P axis and show asymmetric distributions along the A-P axis in the retina far earlier than *Ventroptin* (*3*, *6*). *Ventroptin* misexpression did not alter the expression patterns of these transcription factors (*10*). On the other hand, *SOHo1* and *GH6* do not affect the expression of *ephrin A2* (*6*), which suggests that *Ventroptin* is not controlled by these two factors.

The polarity along the D-V axis in the retina appears to be determined after stage 11 and before stage 13/14 in the chick (*22*, *23*). *BMP-4* and *Ventroptin* expressions are detectable in the optic vesicle from stage 10 or 11 onward (*5*, *10*). Therefore, the counteraction between Ventroptin and BMP-4 appears to determine and maintain the regional specificity along the D-V axis. At E6, when the first retinal axons enter the tectum (*24*), *Ventroptin* shows the nasal high–temporal low gradient expression pattern. From this stage on, Ventroptin seems to control retinotectal projection along the A-P axis by controlling the expression of *ephrin A2*. *BMP-4* is expressed specifically in the dorsal retina, evenly along the A-P axis. At later stages (E6 to 8), expression of *BMP-4* was markedly reduced and was detected only in the peripheral margin of the retina (*10*). Thus, BMP-4 is not likely to be involved in the projection along the A-P axis. On the other hand, we found that Noggin, a structurally unrelated BMP antagonist, had the same activity as Ventroptin in expression of *Tbx5* (*10*), *cVax* (*10*), and *ephrin A2* (Fig. 4B, c; 6 out of 6 embryos), when it was misexpressed in the retina. These results suggest the presence of another member of the TGF-β family in the retina, which binds to Ventroptin (and Noggin) and is involved in retinotectal projection along the A-P axis. Our study thus indicates that BMP family members and Ventroptin are involved in topographic retinotectal projection along the D-V and A-P axes.

References and Notes

1. R. W. Sperry, *Proc. Natl. Acad. Sci. U.S.A.* **50**, 703 (1963).
2. G. A. Hyatt *et al.*, *Development* **122**, 195 (1996).
3. J. Yuasa, S. Hirano, M. Yamagata, M. Noda, *Nature* **382**, 632 (1996).
4. D. Schulte, T. Furukawa, M. A. Peters, C. A. Kozak, C. L. Cepko, *Neuron* **24**, 541 (1999).
5. K. Koshiba-Takeuchi *et al.*, *Science* **287**, 134 (2000).
6. D. Schulte, C. L. Cepko, *Development* **127**, 5033 (2000).
7. R. Suzuki *et al.*, *Mech. Dev.* **98**, 37 (2000).
8. Supplementary Web material is available on *Science* Online at www.sciencemag.org/cgi/content/full/293/5527/111/DC1.
9. H. Suzuki *et al.*, *Nucleic Acids Res.* **24**, 289 (1996).
10. H. Sakuta *et al.*, data not shown.
11. A. J. Kahn, *Dev. Biol.* **38**, 30 (1974).
12. A. T. Dudley, E. J. Robertson, *Dev. Dyn.* **208**, 349 (1997).
13. Chick *Ventroptin* was also expressed in the forebrain and diencephalon (*10*). It was also expressed in limb buds, with similar expression patterns in both the wing and leg buds (*10*). The expression patterns of *Ventroptin* in these organs were also complementary to that of *BMP-4*. Therefore, Ventroptin may also control the morphogenesis of the brain and limbs in cooperation with other BMP-neutralizing factors. *Ventroptin* expression was not detectable in the spinal cord at E8 (*10*).
14. W. C. Smith, *Trends Genet.* **15**, 3 (1999).
15. A. Fainsod, *et al.*, *Mech. Dev.* **63**, 39 (1997).
16. I. L. Blitz, O. Shimmi, K. Wunnenberg-Stapleton, M. B. O'Connor, K. W. Cho, *Dev. Biol.* **223**, 120 (2000).
17. In embryos with misexpressed *Ventroptin*, the dorsonasal axons also projected to the posterior end of the dorsal tectum (3 out of 3 embryos). On the other hand, the ventral axons, in which *Ventroptin* is endogenously expressed at a significant level, projected to the normal places (4 out of 4 embryos) (*10*).
18. H. J. Cheng, M. Nakamoto, A. D. Bergemann, J. G. Flanagan, *Cell* **82**, 371 (1995).
19. B. Monschau *et al.*, *EMBO J.* **16**, 1258 (1997).
20. M. R. Hornberger *et al.*, *Neuron* **22**, 731 (1999).
21. D. Dutting, C. Handwerker, U. Drescher, *Dev. Biol.* **216**, 297 (1999).
22. W. J. Crossland, W. M. Cowan, L. A. Rogers, J. P. Kelly, *J. Comp. Neurol.* **155**, 127 (1974).
23. T. Matsuno, N. Itasaki, H. Ichijo, H. Nakamura, *Neurosci. Res.* **15**, 96 (1992).
24. W. J. Crossland, W. M. Cowan, L. A. Rogers, *Brain Res.* **91**, 1 (1975).

25. We thank S. Takami, M. Gotoh, S. Tsukada, M. Ishida, H. Kuribayashi, and S. Usami for technical assistance and A. Kodama for secretarial assistance. Supported by grants from the Ministry of Education, Science, Sports and Culture of Japan, and from Core Research for Evolutional Science and Technology of the Japan Science and Technology Corporation.

18 December 2000; accepted 4 June 2001

A Transcriptively Active Complex of APP with Fe65 and Histone Acetyltransferase Tip60

Xinwei Cao and Thomas C. Südhof*

Amyloid-β precursor protein (APP), a widely expressed cell-surface protein, is cleaved in the transmembrane region by γ-secretase. γ-Cleavage of APP produces the extracellular amyloid β-peptide of Alzheimer's disease and releases an intracellular tail fragment of unknown physiological function. We now demonstrate that the cytoplasmic tail of APP forms a multimeric complex with the nuclear adaptor protein Fe65 and the histone acetyltransferase Tip60. This complex potently stimulates transcription via heterologous Gal4- or LexA-DNA binding domains, suggesting that release of the cytoplasmic tail of APP by γ-cleavage may function in gene expression.

Amyloid-β precursor protein is a cell-surface protein with a large NH_2-terminal extracellular sequence, a single transmembrane region (TMR), and a short COOH-terminal cytoplasmic tail (*1–4*). The α- and β-secretases initially cleave APP at defined extracellular sequences outside of the TMR. Thereafter, γ-secretase cuts APP in the middle of the TMR to generate small extracellular peptides and an intracellular fragment that is composed of half of the TMR (10 to 12 residues) and the cytoplasmic tail (47 residues). The small secreted peptides include amyloid-β peptides (Aβ40 and Aβ42), which are involved in Alzheimer's disease. γ-Cleavage of APP requires presenilins, intrinsic membrane proteins that are mutated in some cases of familial Alzheimer's disease (*1–5*). In addition to APP, two closely related homologs, APLP1 and APLP2, are expressed in vertebrates and also appear to be cleaved by α- and γ-secretases (*6*). The structures of APP and APLPs resemble cell-surface receptors whose proteolysis may be triggered by an external ligand; indeed, several binding activities of the extra- and intracellular regions of APP have been identified [e.g., see (*7–10*)]. Furthermore, triple knockouts of APP, APLP1, and APLP2 in mice are lethal, suggesting that these proteins are essential (*11*). However, the function of APP and APLPs, and of their proteolytic cleavages, remains unclear. Clues to such a function come from

The Center for Basic Neuroscience, Department of Molecular Genetics, and Howard Hughes Medical Institute, The University of Texas Southwestern Medical Center, Dallas, TX 75390–9111 USA.

*To whom correspondence should be addressed. E-mail: Thomas.Sudhof@UTSouthwestern.edu